Emergent Materials (2025) 8:667–687
https://doi.org/10.1007/s42247-024-00808-9

ORIGINAL ARTICLE

A study on the temperature-dependent impedance spectroscopic measurements of barium titanate mixed with Mg^{2+}/Ca^{2+} modified barium hard-type ferrite

Yassine Slimani[1] · Bayram Ünal[2] · Abdulhadi Baykal[3] · Munirah A. Almessiere[1,4] · Atul Thakur[5] · Khalid Mujasam Batoo[6]

Received: 13 March 2024 / Accepted: 20 July 2024 / Published online: 8 August 2024
© Qatar University and Springer Nature Switzerland AG 2024

Abstract
In this work, $(BaTiO_3)_{1-x}$ – $(Ba_{0.96}Mg_{0.02}Ca_{0.02}Fe_{12}O_{19})_x$ (where $0.0 \leq x \leq 1.0$) composite ceramics, abbreviated $(BTO)_{1-x}$ – $(BaMgCaFeO)_x$ were prepared. The successful formation of the composites was confirmed via XRD, FE-SEM, and EDX techniques. No additional phases were identified. The surface morphology observation showed large-sized grains with platelet shapes associated with the BaMgCaFeO hexaferrite phase and smaller spherical grains associated with the BTO phase. The electrical and dielectric properties have been investigated. Impedance spectroscopy was employed to explore key parameters including ac conductivity, activation energy, dielectric constant, dielectric loss, dissipation factor, real/imaginary impedance, and Cole-Cole impedance analysis. Measurements spanned 40 to 120 °C, encompassing frequencies up to 3.0 MHz. Notably, ac conductivity adhered to the power law frequency rule for all ratios across transition temperatures. Activation energy calculations (47 to 357 meV) varied due to composition and transition temperature changes, evident in distinct two-region patterns in Arrhenius plots. Dielectric parameters exhibited considerable variation across frequency, temperature, and ratio, with unique trends for each ratio attributed to intra-grain, grain boundary effects, and ionic contributions. Changes in activation energy and dc conductivity, across ratios, stemmed from multiple conduction mechanisms, including electron hopping and ionic contributions. Cole-Cole impedance functions exhibited diverse profiles of straight lines and semicircles, dependent on temperature and ratios, emphasizing complex capacitive and resistive responses influenced by intra-grains, grain boundaries, and binary ions within the composites.

Keywords $BaTiO_3$ · Barium hexaferrite · Dielectric properties · Ac/dc conductivity · Impedance spectroscopy

✉ Yassine Slimani
yaslimani@iau.edu.sa; slimaniyassine18@gmail.com

[1] Department of Biophysics, Institute for Research and Medical Consultations (IRMC), Imam Abdulrahman Bin Faisal University, P.O. Box 1982, Dammam 31441, Saudi Arabia

[2] Institute of Forensic Sciences and Legal Medicine, İstanbul University-Cerrahpaşa, Büyükçekmece Campus, Büyükçekmece-İstanbul 34500, Turkey

[3] Food Engineering Department, Faculty of Engineering, Istanbul Aydin University, Florya-Istanbul 34295, Turkey

[4] Department of Physics, College of Science, Imam Abdulrahman Bin Faisal University, P.O. Box 1982, Dammam 31441, Saudi Arabia

[5] Centre for Nanotechnology, Amity University Haryana, Gurugram 122413, India

[6] King Abdullah Institute for Nanotechnology, King Saud University, P.O. Box-2455, Riyadh 11451, Saudi Arabia

1 Introduction

There is a continuous need for novel products with novel and superior multifunctional practical characteristics. Therefore, in order to guarantee their broad range of applications, engineering materials need to possess robust and adaptable features. In recognition of their advantageous multifunctional features, particularly polarization in the magnetic field and magnetization in the electric field, dielectric-magnetic composites have recently attracted a lot of attention from the scientific community. This new class of materials offers the opportunity to control the magnetization by applying an electric field and the polarization by a magnetic field in one system [1]. Moreover, these composites are endowed with a high permittivity as well as strong ferroelectric and magnetic aptitudes which can be achieved even at room

temperature [2]. Such multifunctional materials have a great potential to be used in various technological applications including magnetic field probes, sensors, microwave devices, actuators, energy harvesting, capacitive-inductive passive filters for communications, random access memories, magneto-electric transducers, microwave phase shifters, and so on [3, 4].

Several investigations studying the characteristics of dielectric-magnetic composites are based on dielectric perovskite titanates and magnetic spinel ferrites, which have been widely described in the literature. According to a review of the literature, lead zirconate titanate ($PbZr_xTi_{1-x}O_3$ or PZT)-based composite materials possess elevated multiferroic properties [5]. Yet, the utilization of lead (Pb) based products is prevented since their production releases harmful chemicals into the surrounding environment. Hence, reduced utilization of Pb-based supplies is necessary due to environmental concerns. Thus, products devoid of Pb and with good dielectric characteristics have emerged as a viable substitute for PZT. Given this, Pb-free barium titanate ($BaTiO_3$ or BTO) has been involved as an alternative. With ABO_3 perovskite structure, $BaTiO_3$ material is recognized for its excellent ferroelectric properties and exhibits remarkable dielectric behaviors and electrical properties (including *ac* and *dc* conductivity) due to its polarization capabilities, high dielectric constant, and significant dielectric loss under the influence of an alternating electric field, etc. [6]. These properties, in addition to its chemical stability, render BTO a crucial element in many applications including capacitors, piezoelectric devices, and memory applications as well as one of the best combinations of dielectric-magnetic composites. On the other hand, magnetic spinel ferrites are one of the ideal candidates for designing new dielectric-magnetic composites based on $BaTiO_3$ [7]. Among many spinel oxides, cobalt ferrite ($CoFe_2O_4$), nickel ferrite ($NiFe_2O_4$), and zinc ferrite ($ZnFe_2O_4$), either in undoped or doped forms and in simple or mixed forms, are some of the candidates that are used to develop new dielectric-magnetic composites. This is attributed to their interesting magnetic and electrical properties that could be easily adjusted to address the competing demands of dielectric-magnetic composites for specific multifunctional applications. The unique properties arising from the synergistic combination of the distinct components of dielectric perovskite $BaTiO_3$ and magnetic spinel ferrites offer unprecedented opportunities for tailoring both the electrical and magnetic characteristics to specific requirements. Exploring the electrical and dielectric properties of the dielectric perovskite $BaTiO_3$ and spinel ferrites composites across varying composition ratios holds promise for advancements in electronics, telecommunications, energy, and beyond. Some studies reported that the rise in the concentration of magnetic spinel ferrite phase negatively influences the magneto-electric response, however, a vigilant selection of ferrite chemical composition, in addition to the attentive adoption of preparation procedure could help in overcoming some of the negative effects [7]. For instance, $CoFe_2O_4$ is a well-known spinel ferrite material that displays ferromagnetic properties and good magnetostrictive characteristics, which are greatly affected by the microstructural changes and the degree of cation inversion [8]. Accordingly, numerous $BaTiO_3$-$CoFe_2O_4$ composites showed superior ferroelectric, ferromagnetic, and magnetoelectric characteristics and have been broadly investigated experimentally and theoretically [9–11]. D. Bochenek et al. [12] studied the properties of $BaTiO_3$-$Ni_{0.64}Zn_{0.36}Fe_2O_4$ multiferroic composites. The prepared composite ceramics displayed multiferroism at ambient temperature, low dielectric loss, and high permittivity. The magnetic features are found to be greatly dependent on the content of the spinel ferrite phase. The researchers reported that the enhanced group of multifunctional characteristics permits the expansion of the potential of exploiting these composites in microelectronics. Many other researchers have also reported the production of BTO-spinel ferrite-based composites like Ca-doped $BaTiO_3$-La-doped Ni-Zn ferrite systems [13], $BaTiO_3$- $NiFe_2O_4$ composites [5], $BaTiO_3$-$Mg_{0.7}Cd_{0.3}Fe_2O_4$ ceramic composites [14], $(1-x)(Ba_{0.88}Sr_{0.1}Ca_{0.02})(Ti_{0.95}Zr_{0.05})O_3$–$x(Ni_{0.9}Mg_{0.1})Fe_2O_4$ composite ceramics [15], $BaTiO_3$/$CoFe_{1.98}Nb_{0.02}O_4$ systems [16], $BaTiO_3$/$(Co_{0.8}Ni_{0.1}Mn_{0.1}Fe_{1.9}Ce_{0.1}O_4)_x$ composites [17].

To the best of our knowledge, there is a large number of studies on $BaTiO_3$ and spinel ferrite composites, however, studies on $BaTiO_3$ and hexaferrite composites are lesser reported in the literature. Unfortunately, although magnetic hexaferrite materials have gained considerable interest during the last decades, there are still few studies on composites made up of dielectric BTO phase and hexaferrite phase. Hexaferrites have witnessed considerable attention due to their both peculiar magnetic and ferroelectric features including superior saturation magnetization, large coercivity, strong anisotropy, high electrical resistivity, low dielectric constant, superior chemical stability, and good thermal stability, making them suitable for magnetic recording, permanent magnets, and microwave applications [18]. In particular, Ba-hexaferrites ($BaFe_{12}O_{19}$) are M-type hexaferrites with a space group P63/mmc and a magnetoplumbate structure. They are very attractive ferromagnetic materials with important magnetostrictive and piezomagnetic properties [19]. Their superior crystal anisotropy increases their use as magnetic materials while their narrow bandwidth energy makes them required for active photocatalytic applications [20].

Some investigations on dielectric BTO and Ba-based hexaferrite composites were reported in the literature. For instance, A. Kumari et al. [21] prepared BTO-$BaFe_{12}O_{19}$ composites via a solid-state reaction route. The real part of permittivity (ε') was raised and the dielectric loss (tanδ) was diminished with increasing Ba-hexaferrite concentration. It is proposed that hopping conduction and space charge are key factors in raising the permittivity. Additionally, a rise in the energy of activation is shown in direct proportion to the amount of the hexaferrite phase. N. Hooda et al. [22] fabricated BTO-$BaFe_{12}O_{19}$ composites by solid-state reaction with increased dielectric constant in comparison to sole phases. At low frequencies and high temperatures, there was a dispersion in both the dielectric constant and tangent loss. BTO-$BaFe_{12}O_{19}$ composites were also prepared by Z. Dong et al. [23]. As the amount of $BaFe_{12}O_{19}$ increased, the electrical conductivity and relative permittivity rose. The significant influence of space charges on the composite ceramics was responsible for this increment.

Numerous studies demonstrated that the physical, electric, and magnetic properties of Ba-hexaferrite materials can be altered by substituting the cations at Fe and/or Ba sites, thus allowing to the achievement of the desired physicochemical properties. Accordingly, some dielectric BTO and doped Ba-hexaferrite composites were reported. For instance, M.M. Salem et al. [24] prepared composite ceramics made of BTO and Al-doped $BaFe_{12}O_{19}$ ($BaFe_{11.9}Al_{0.1}O_{19}$) through the solid-state reaction technique. The structure, morphology, magnetic, and dielectric characteristics were systematically investigated. All prepared ceramics display simultaneously ferromagnetic and ferroelectric responses. Furthermore, it was reported that the electrical characteristics of ceramic composites, greatly depend on the compositional ratios, which influence the microstructural features. In another study, A. Kumari et al. [25] investigated the properties of (1-x)$BaTiO_3$–(x)$Ba_{0.9}Ca_{0.1}Fe_{12}O_{19}$ composite ceramics produced via standard solid-state reaction method. The dielectric constant was reported to increase as the Ca-doped Ba-hexaferrite content increased. The composite ceramics also revealed typical dielectric dispersive behavior as a function of frequency. AC conductivity was found to increase with the rise in the concentration of $Ba_{0.9}Ca_{0.1}Fe_{12}O_{19}$. Moreover, Zi-Yan Gao et al. [26] investigated the properties of ceramic composites made of $BaTiO_3$ and Mn-doped Ba-hexaferrite ($BaFe_{12-x}Mn_xO_{19}$). In their study, 0.8BTO–0.2$BaFe_{12-x}Mn_xO_{19}$ composites were synthesized via microwave-hydrothermal and microwave-sintering approaches. The dielectric constant and the resistivity of the composite ceramics were reported to increase with the increase in Mn content, whereas the dielectric loss decreased.

Doping/substituting the cations at Fe and/or Ba sites could hence alter the physical, electric, and magnetic properties of Ba-hexaferrite materials, which can allow the achievement of desired physicochemical properties needed for superior dielectric-ferrite composites based on BTO and hexaferrite phases. Recently, Ca-doped $BaFe_{12}O_{19}$ samples have been fabricated via a sol-gel auto-combustion approach [27]. The insertion of Ca enhanced the saturation magnetization (M_s)and the remanence (M_r) and reduced the coercive field (H_c). Ca-doped $BaFe_{12}O_{19}$ are also produced by I. Ali et al. [28] in which H_c and electrical resistivity enlarged. Another study reported that the introduction of Mg ions in Ba-hexaferrite lowered the impedance and raised the larger conductivity [29]. The co-incorporation influence of Mg and Ca ions on the characteristics of Ba-hexaferrite (henceforth referred to as BaMgCaFeO) was examined in an investigation conducted by Y. Slimani's research team [30]. The produced materials exhibited ferrimagnetism and other intriguing features. Smaller doping amounts were shown to be beneficial for improving M_s and M_r values, wherein the greatest values were seen for $Ba_{0.96}Mg_{0.02}Ca_{0.02}Fe_{12}O_{19}$ composition. On the other hand, co-doping decreased H_c. By integrating the interesting $Ba_{0.96}Mg_{0.02}Ca_{0.02}Fe_{12}O_{19}$ material with $BaTiO_3$ to form dielectric-ferrimagnetic composites, one aims to harness their combined characteristics to engineer novel functionalities and enhance device performance. Based on these findings, the current work concerns a study of the dielectric and electric properties of the perovskite-hexaferrite composites consisting of BTO-BaMgCaFeO. This exploration seeks to investigate the intricate electrical and dielectric properties of $(BTO)_{1-x}$ – $(BaMgCaFeO)_x$ composites, as these properties evolve across varying composition ratios. Through a systematic analysis of how different composition levels influence electrical behaviors, dielectric constants, loss tangents, activation energies, and complex impedance profiles, one can uncover the intricate relationship between composition, crystallite structure for intra-grains, and electrical performance. By revealing the dynamic relationship between composition and electrical characteristics, this research aims to contribute to the growing understanding of how these nanocomposites can be tailored to drive innovation in fields such as electronics, energy harvesting, and advanced communication systems. The goal is to unlock new avenues for customizing these composites to fulfill specific application requirements in cutting-edge technologies.

2 Experimental

$(BTO)_{1-x}-(BaMgCaFeO)_x$ $(0.0 \le x \le 1.0)$ composite ceramics were fabricated. The first stage consists of preparing the BTO material by using as starting materials $BaCO_3$ and $Ti[OCH(CH_3)_2]_4$. Two solutions of Ba citrate and Ti precursor were created by dissolving the starting materials in ethanolic solutions by means of a magnetic stirrer. The Ti precursor solution was stirred at a temperature of 80 °C. After a while, the two solutions were blended, and under continuous stirring and heating a gel was generated. The obtained BTO phase was placed overnight in a drying oven at 120 °C and afterward calcined at 600 °C. In the second stage, $Ba_{0.96}Mg_{0.02}Ca_{0.02}Fe_{12}O_{19}$ hexaferrite was fabricated via sol-gel route. Based on the mentioned stoichiometry, different nitrates of $Fe(NO_3)_2 \cdot 9H_2O$, $Mg(NO_2)_3$, $Ca(NO_2)_3$, and $Ba(NO_3)_2$ were dissolved and mixed in deionized water until the achievement of a homogenous and clear solution. This mixture is kept stirring at 80 °C. Citric acid and ammonia solution were added to act as fuel and adjust the pH value to 7, respectively. The temperature was increased close to 250 °C and kept under stirring until a self-ignition was generated. The formed black powder is sintered at 1100 °C for 5 h. In the last stage, the fabricated BTO and BaMgCaFeO samples were blended together into the forms of disks by means of the solid-state reaction method, a binder like polyvinyl alcohol, and a hydraulic press. The different prepared composite ceramics are $(BTO)_{1-x}-(BaMgCaFeO)_x$ $(0.0 \le x \le 1.0)$ composite ceramics. The created disks are sintered at 1300 °C for 4 h. The structural characteristics of produced ceramics were examined using an X-ray diffractometer (XRD; Rigaku MiniFlex 600) using CuKα radiation. The surface morphology and chemical compositions were examined using a field emission scanning electron microscopy (FE-SEM; FEI Quanta) equipped with an EDX spectroscopy. An impedance analyzer (Novocontrol Technologies) was used to measure the electrical and dielectric properties across a broad range of frequencies.

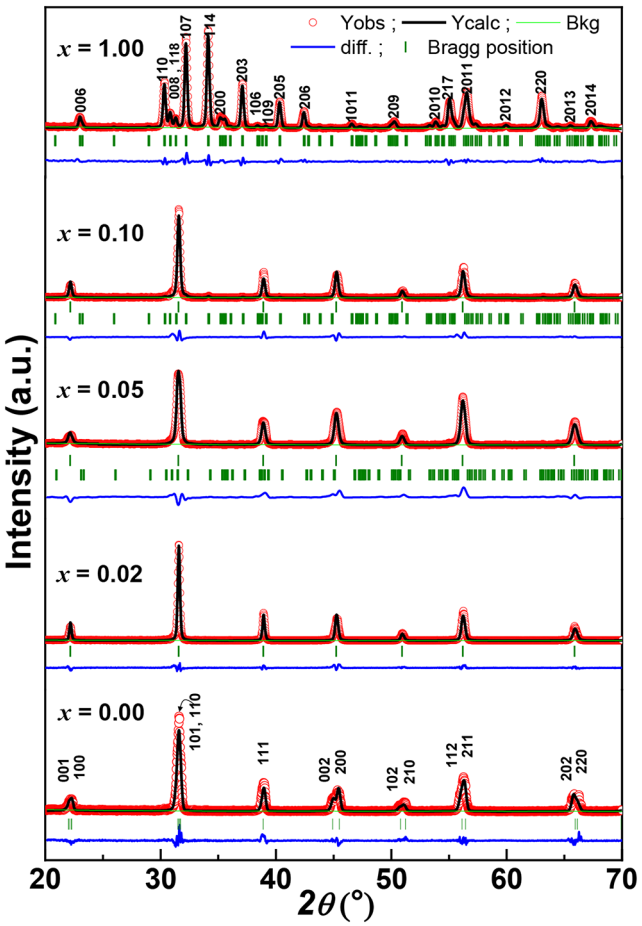


Fig. 1 XRD patterns of $(BTO)_{1-x}-(BaMgCaFeO)_x$ $(0.0 \le x \le 1.0)$ ceramic composites

3 Results & discussion

3.1 Microstructure & morphology

Figure 1 presents the experimental and refined XRD results for $(BTO)_{1-x}-(BaMgCaFeO)_x$ $(0.0 \le x \le 1.0)$ ceramic composites. The phase identification was performed via Match 3, while the Rietveld refinement was carried out by means of the FullProf program. In Fig. 1, the abbreviations Yobs, Ycal, Bkg, Diff., and Bragg position designate the observed (experimental) XRD data, calculated XRD profile, background, difference line between the observed and calculated XRD profiles (Yobs – Ycal), and the position of Bragg reflection peaks, respectively. The refinement goodness factors (R-Bragg and χ^2), crystal structures, space groups, and phase fractions are listed in Table 1. The graphic displays also the *hkl* values of the significant peaks. The ceramic with $x = 0.0$ reveals Bragg reflection positions belonging to only the tetragonal $BaTiO_3$ phase (space group $P4mm$), which are indexed using the ICDD card no. 96–901–4669. The splitting observed in the peak positioned around 45° is characteristic of the tetragonal phase for BTO material. The ceramic with $x = 1.00$, on the other hand, contains Bragg reflections (ICDD card no. 96-100-8329) corresponding to only the hexagonal Ba-based ferrite phase with a space group of $P63/mmc$. Both pristine BTO and BaMgCaFeO are free of impurities. The various peaks in the case of $(BTO)_{1-x}-(BaMgCaFeO)_x$ composite ceramics ($x = 0.05$ and 0.10) are solely attributed to the hexagonal BaMgCaFeO phase and the pseudo-cubic BTO phase (space group $Pm\text{-}3m$), based on the ICDD card numbers 96-100-8329 and 96-150-7758, respectively. When the BaMgCaFeO phase was combined with the BTO phase, the splitting observed in the peaks of the tetragonal BTO phase combined into single

Table 1 Rietveld refinement parameters of $(BTO)_{1-x}-(BaMgCaFeO)_x$ $(0.0 \le x \le 1.0)$ ceramic composites

x content (%)	0.00	0.02	0.05	0.10	1.00
Crystal structure					
BTO phase	Tetragonal	Cubic	Cubic	Cubic	--
BaMgCaFeO phase	--	--	Hexagonal	Hexagonal	Hexagonal
Space group					
BTO phase	*P4mm*	*Pm-3 m*	*Pm-3 m*	*Pm-3 m*	--
BaMgCaFeO phase	--	--	*P63/mmc*	*P63/mmc*	*P63/mmc*
Phase fractions					
BTO phase	100%	100%	96.2%	91.3%	--
BaMgCaFeO phase	--	--	3.8%	8.7%	100%
Fitting parameters					
R-Bragg	9.93	7.22	14.08	10.2	6.5
χ^2	1.66	2.30	1.72	2.1	0.5

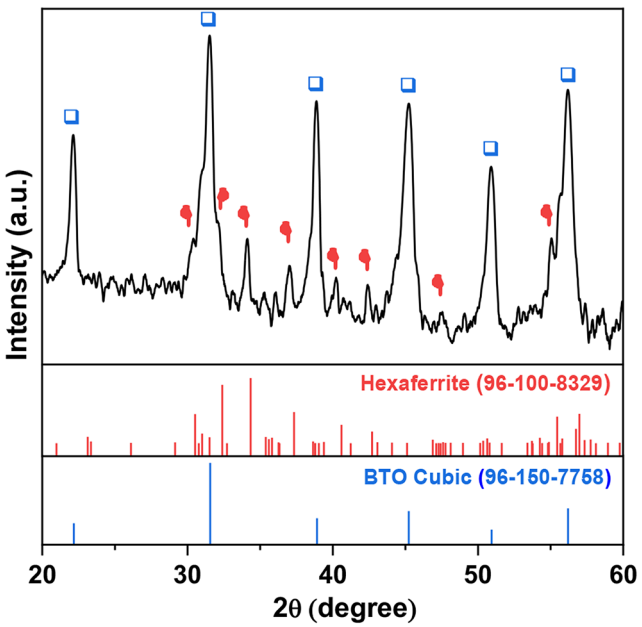


Fig. 2 A semi-logarithmic scale XRD pattern of $(BTO)_{0.9}$–$(BaMgCaFeO)_{0.1}$ ceramic composite

peaks, indicating a phase transition from the tetragonal to the cubic structure. It is worth noting that no other peaks are identified, which indicates that no chemical reaction has occurred between the two phases and the different ceramic composites are of high purity.

Peaks associated with the BaMgCaFeO phase were not clearly seen at low concentration ($x = 0.02$) due to the compressed XRD graphs as well as the low concentration of additive, which is mostly below the detection limit of XRD instrument. Accordingly, a semi-logarithmic scale XRD pattern for the $(BTO)_{0.9}$–$(BaMgCaFeO)_{0.1}$ ceramic composite (i.e., $x = 0.1$) is presented in Fig. 2 for better clarity regarding the presence of the two phases. As shown in this figure, it is obvious that the different peaks are linked to the magnetoplumbite hexagonal BaMgCaFeO phase (□ symbol) and the pseudo-cubic BTO phase (□ symbol). The single peak around 45° is characteristic of the cubic phase for BTO material. The ICDD card numbers for BaMgCaFeO and BTO phases are 96-100-8329 (red lines) and 96-150-7758 (blue lines), respectively. There were no other peaks identified, which indicates that no chemical reaction has occurred between the two phases.

Figure 3**(a)** presents the FE-SEM micrographs, wherein grains with two distinct geometries exist in the composite ceramic. The EDX analyses were performed in different regions on the sample surface. For instance, the region indicated with a red multiplication sign in Fig. 3**(a)** revealed very high intensity peaks of iron (Fe) element. However, the concentration of Fe element is very negligible in the region indicated with a yellow multiplication sign Fig. 3**(a)**. Furthermore, the intensity of Ba and Ti elements become more intense in this region in comparison to the first region. As endorsed by EDX analyses (Fig. 3**(b) and 3(c)**), the large-sized grains with platelets-shapes are mainly associated with the hexaferrite BaMgCaFeO phase, while the smaller spherical grains are mainly associated with the BTO phase. The sintering process at a high temperature would drive a diffusion mechanism, leading to the blending of BaMgCaFeO grains and hence the enlargement in the size of BaMgCaFeO grains [31].

3.2 Electrical and dielectric analyses

The electrical and dielectric properties of ferroelectric-ferrimagnetic composite ceramics represent one of the most important properties of its composites. Such properties have some important multi-ferroic potentials in various applications such as ceramic capacitors, humidity and gas sensors, and some active and multifunctional devices due to their relatively high dielectric parameters even at room temperature [32–34]. In order for such nanocomposites to be preferred as a comprehensive circuit element, it is desired that both electrical and dielectric parameters can be measured by existing methods and be sensitive to independent variables such as frequency, temperature, and composition ratio. Consequently, the electrical and dielectric parameters of the $(BTO)_{1-x}-(BaMgCaFeO)_x$ $(0.0 \le x \le 1.0)$ composite

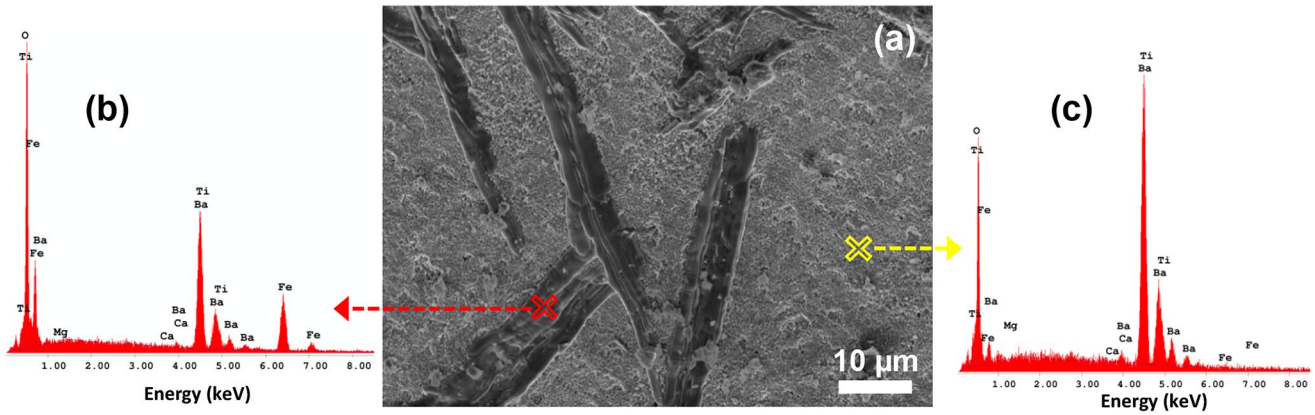


Fig. 3 **(a)** FE-SEM micrograph and **(b**, **c)** EDX spectra of $(BTO)_{0.9}$–$(BaMgCaFeO)_{0.1}$ ceramic composite

ceramics such as ac/dc conductivity, activation energy, dielectric constant/loss, dissipation factor, real/imaginary impedances, and Nyquist analysis of Cole-Cole plots of complex impedances were evaluated as functions of both frequencies up to 3.0 MHz at temperatures between 40 °C and 120 °C and for the composition ratios of 0.0 ≤ x ≤ 1.0.

3.3 Ac conductivity

The phenomenon of conductivity is conventionally understood as the consequence of the displacement of mobile charge carriers leading to alterations in the electric field, thereby influencing the underlying mechanisms that contribute to the overall conductivity. In light of this, the formulation of *ac* conductivity can be articulated in the subsequent manner [35]:

$$\sigma_{ac}(\omega, x) = \omega \epsilon_o \epsilon'(\omega, x) tan\delta(\omega, x) \quad (1)$$

In this expression, $\epsilon'(\omega, x)$ signifies the relative permittivity, ϵ_0 represents the absolute permittivity, *tanδ(ω,x)* denotes the dissipation factor, ω corresponds to the angular frequency, and x pertains to the composition ratio.

The behavior of *ac* conductivity of composites is usually influenced by factors such as the composition, structure, intra-grains, grain boundaries, and defects, and temperature. The *ac* conductivity of BTO can be understood through its polarization and depolarization processes. The *ac* conductivity of BTO is also frequency-dependent, meaning it changes with the frequency of the alternating electric field. At lower frequencies, BTO can exhibit relatively low *ac* conductivity due to slower polarization processes. As the frequency increases, the ability of the material to respond to the changing field direction improves, leading to increased *ac* conductivity. This frequency-dependent behavior is often represented by the "Cole-Cole" plot, which shows the relationship between real and imaginary parts of complex impedance. Binary ion-substituted Ba-hexaferrites, with ions like Ca^{2+} and Mg^{2+} ions substituted for Ba^{2+} ion, can have varying *ac* conductivity behaviors depending on the specific composition and structure. The *ac* conductivity of the $(BTO)_{1-x}$ – $(BaMgCaFeO)_x$ $(0.0 \le x \le 1.0)$ composite ceramics can hence exhibit frequency-dependent behavior as well, but the underlying mechanisms might differ from those in ferroelectric materials like BTO composites. Accordingly, the 3D representation of *ac* conductivity in the context of the $(BTO)_{1-x}$ – $(BaMgCaFeO)_x$ $(0.0 \le x \le 1.0)$ composite ceramics is illustrated in Fig. 4. This presentation shows the interaction of frequency and temperature in various composition ratios. The observed conductivity patterns offer insights into the underlying conduction mechanisms across various compositional arrangements and temperature conditions.

In the case of pure BTO ($x = 0$), the closely adherent adherence of conductivity to the power law frequency dependency across the entire temperature spectrum up to 120 °C suggests a predominant conduction mechanism characterized by frequency-dependent charge carrier dynamics. However, the presence of discernible fluctuations at lower temperatures indicates that the conduction process becomes intricate under these specific thermal conditions. These fluctuations may be attributed to localized charge carrier mobility variations influenced by lattice defects, crystallite imperfections, grain size effect, or other factors, suggesting a complex interplay of these elements in the overall conduction process. For the pure BaMgCaFeO ceramic ($x = 1$), a comparable deviation from the anticipated conduction behavior is evident. The relevant graph demonstrates an initial distortion in the conduction mechanism, suggesting the influence of factors like defect-related effects or interface interactions. Beyond this initial distortion, the graph reveals the existence of two distinct regions characterized by separate exponential power-law behaviors. This distinctive contrast in behavior points toward the presence of intricate and

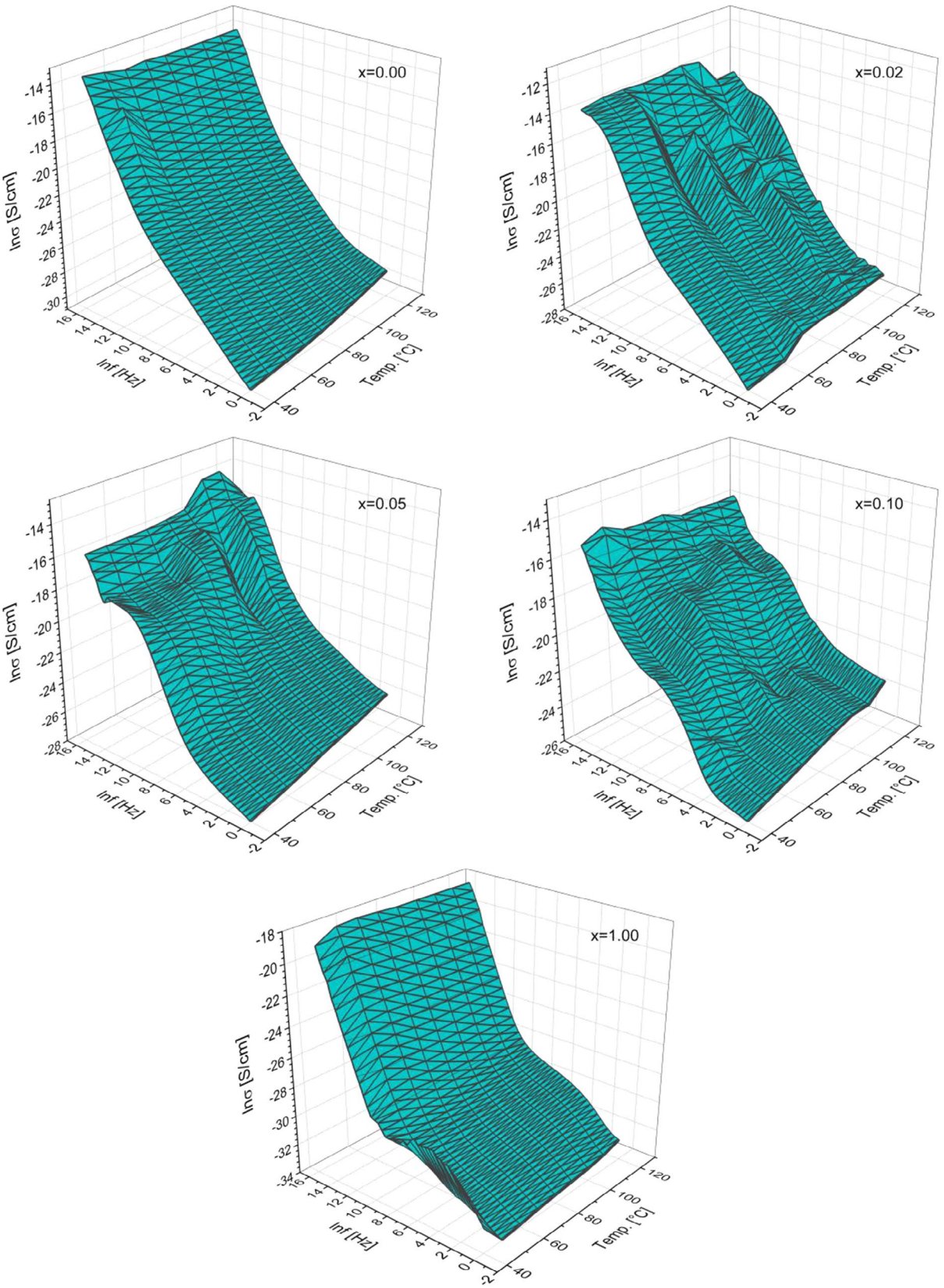


Fig. 4 The 3D representation of ac conductivity of $(BTO)_{1-x}$ – $(BaMgCaFeO)_x$ $(0.0 \leq x \leq 1.0)$ composite ceramics as functions of frequency and temperature

possibly multi-step conduction pathways within the BaMgCaFeO composites at varying temperature regimes.

In the context of $(BTO)_{1-x}$ – $(BaMgCaFeO)_x$ $(0.0 \leq x \leq 1.0)$ composite ceramics with composition ratios of x = 0.02, 0.05, and 0.10, a diverse array of trends emerges as frequency is modulated across the temperature spectrum up to 120 °C. Specifically, it is evident that at lower frequencies, the conductivity displays a positive correlation with increasing temperatures, indicating enhanced conduction efficiency with elevated thermal energy. In contrast, at higher frequencies, the conductivity behavior exhibits fluctuations in response to temperature changes across all $(BTO)_{1-x}$ – $(BaMgCaFeO)_x$ $(0.0 \leq x \leq 1.0)$ composite ceramics. This intriguing behavior suggests the existence of intricate interactions between frequency and temperature, potentially originating from dynamic charge carrier responses, localized polarization effects, or interfacial dynamics. The intricate nature of these interactions underscores the complicated interactions between the constituents and their respective conductivity mechanisms. However, the fluctuations observed at higher frequencies underline a more intricate relationship between frequency and temperature. This phenomenon suggests that higher-frequency charge carrier dynamics are influenced by a combination of factors, including thermal energy and the inherent properties of the nanocomposite constituents. The presence of fluctuating trends along the frequency axis underscores the complexity of the conductivity response within the $(BTO)_{1-x}$ – $(BaMgCaFeO)_x$ $(0.0 \leq x \leq 1.0)$ composite ceramics. These fluctuations highlight the intricate interactions between compositional ratios, temperature, and frequency in shaping ac conductivity behavior within the nanocomposite system. Overall, the observed patterns suggest that the conductivity mechanisms within these nanocomposites are multifaceted, involving various charge carrier processes influenced by temperature, frequency, and the interaction between BTO and BaMgCaFeO constituents.

The phase transition of BTO compounds plays a significant role in their *ac* conductivity properties. BTO undergoes a ferroelectric phase transition at a critical temperature, where it transforms from a paraelectric phase to a ferroelectric phase. This transition is accompanied by changes in polarization, dielectric constant, and conductivity of composite ceramics. Below the critical temperature, in the ferroelectric phase, BTO exhibits spontaneous polarization and grain structure. These polar domains can align in response to an applied electric field, leading to enhanced electrical conductivity due to the increased mobility of charge carriers along the grain boundaries. This phenomenon is known as grain wall conduction and contributes significantly to the *ac* conductivity of BTO below the critical temperature. Above the critical temperature, BTO transits into the paraelectric phase, where it loses its spontaneous polarization. In this phase, the conductivity of composite ceramics typically decreases due to the absence/reduction of grain (domain) wall conduction [36]. When BTO is incorporated into a composite material, its properties can interact with those of the other components, leading to complex behavior in terms of electrical conductivity. For instance, the presence of BTO in a composite can influence the distribution of electric fields within the composite ceramics, affecting the movement of charge carriers and thus altering the overall *ac* conductivity. Additionally, interactions between BTO nanoparticles and the matrix material can create interfaces with unique electrical properties, further influencing the conductivity of composite ceramics. Moreover, the morphology and dispersion of BTO particles within the composite can affect the connectivity of conducting pathways and the efficiency of charge transport mechanisms, thereby impacting the *ac* conductivity behavior. Therefore, the phase transition of BTO compound significantly influences the *ac* conductivity properties of the composite.

3.4 Dc conductivity and activation energy

The *dc* conductivity refers to the ability of a material to conduct an electric current under the influence of a steady or direct electric field. Activation energy is a parameter that describes the energy barrier that charged carriers (e.g., electrons or ions) must overcome to move through a material and contribute to its conductivity. The *dc* conductivity is often influenced by the movement of charge carriers, such as electrons or ions, through the grain/grain boundary or crystallite lattice. These charge carriers can be generated by defects, impurities, or thermal excitation. The activation energy refers to the energy required to enable these charge carriers to move. As charge carriers move through the crystallite lattice, they encounter energy barriers due to interactions with lattice vibrations and other lattice defects. The activation energy quantifies the height of these barriers. The activation energy for *dc* conductivity can vary depending on factors such as temperature and the density of charge carriers. The *dc* conductivity and activation energy of $(BTO)_{1-x}$ – $(BaMgCaFeO)_x$ $(0.0 \leq x \leq 1.0)$ composite ceramics depend on the specific compositional ratio, grain/grain boundary, crystallite structure in grains, and defect concentration. These materials are often more associated with their magnetic properties, but their electrical behavior can still be relevant.

The experimental σ_{ac} as a function of frequency can be expressed by the Jonscher's power law of the universal dielectric response (UDR) model [37, 38]:

$$\sigma_{ac} = \sigma_{dc} + A\omega^{n} \tag{2}$$

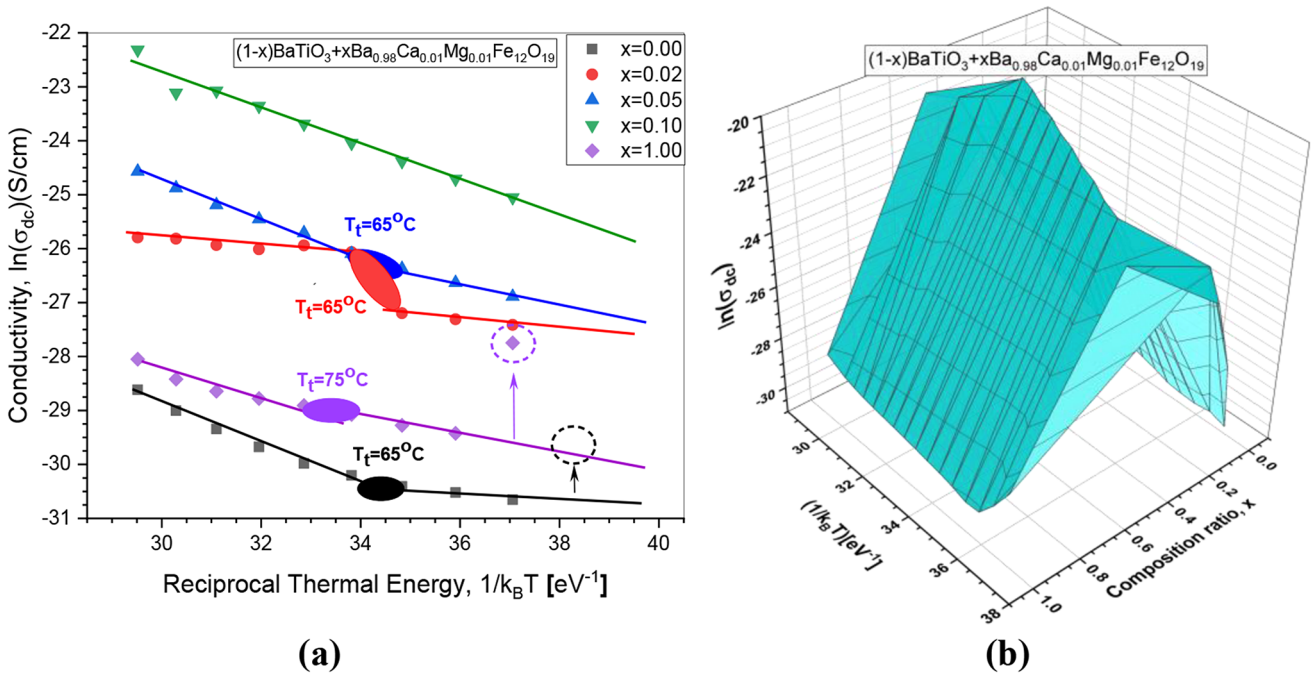


Fig. 5 **(a)** 2D and **(b)** 3D representation of Arrhenius plot of *dc* conductivity of $(BTO)_{1-x}$ – $(BaMgCaFeO)_x$ $(0.0 \le x \le 1.0)$ composite ceramics

Table 2 Activation energy of $(BTO)_{1-x}$ – $(BaMgCaFeO)_x$ $(0.0 \le x \le 1.0)$ composite ceramics measured between 40 and 120 °C

x	E_a (meV)	
	T_{Hi}	T_{Lo}
0.00	357	47
0.02	81	98
0.05	353	182
0.10	330	
1.00	286	176

where σ_{dc} is *dc* conductivity, A is a constant that governs the strength of polarizability, and the exponent n is indicates the interaction degree between the lattice and the ions. The values of *dc* conductivity of the present studied $(BTO)_{1-x}$ – $(BaMgCaFeO)_x$ $(0.0 \le x \le 1.0)$ composite ceramics are estimated from the plateau region in the 3D plots of $log(\sigma_{ac})$ versus $log(f)$ by the linear fitting at lower frequencies. In numerous ferrite composites, the correlation between *dc* conductivity and temperature, often elucidated through an Arrhenius equation, can be mathematically represented as follows [39, 40]:

$$\sigma_{dc}(T,x) = \sigma_o(x)\exp\left(-\frac{E_a(x)}{k_B T}\right) \quad (3)$$

In this expression, E_a symbolizes the activation energy associated with conduction (measured in electron Volts, eV) and k_B signifies the Boltzmann constant. Additionally, x represents the composition ratio, and T denotes the temperature in Kelvin (K). The Arrhenius plots are illustrated in both 2D (Fig. 5**(a)**) and 3D (Fig. 5**(b)**) representations, which will provide a comprehensive understanding of the complex behavior observed across various composition ratios $(0.0 \le x \le 1.0)$. The values of activation energy across the composition ratios are summarized in Table 2.

A distinct feature observed in the activation energy values across the different samples is the presence of two values for most cases, with one above and another below the transition temperatures (T_C), typically ranging between 65 and 75 °C. This bimodal distribution of activation energy is indicative of a dynamic conduction mechanism that varies across these temperature ranges, which are influenced by the specific composition ratios of the nanocomposites. It is notable that x = 0.10 lacks a clear transition temperature, resulting in a consistent activation energy value of 330 meV for all examined temperatures. This can be attributed to the absence of a distinct phase transition in this composition. The comparison of activation energy values above and below the transition temperatures for the various samples reveals intriguing trends. For most composition ratios, the activation energy on the high-temperature side is significantly higher than that on the low-temperature side, with the exception of x = 0.02. This asymmetry in activation energy values suggests a substantial shift in the dominant conduction mechanisms as the temperature increases, with more energy required to facilitate charge transport at higher temperatures. Notably, the presence of a single scattered data point in the *dc* conductivity of BaMgCaFeO ceramic $(x = 1)$ can be attributed to imperfections or anomalies in

the nanocomposite structure, leading to localized fluctuations in the conductivity behavior. The distinctive patterns in the 3D representation of the Arrhenius *dc* conductivity plot highlight the presence of a maximum value across the composition ratios, indicating optimal conductivity at specific compositional arrangements. The notable disparity in activation energies between BTO below and above the transition temperature reflects significant shifts in the underlying conduction mechanisms associated with the phase transition. In contrast, the minimal difference in activation energies for BaMgCaFeO hexaferrite under similar conditions suggests a more stable conduction mechanism, less influenced by temperature-induced changes. The intriguing behavior observed for $x = 0.02$, wherein the *dc* conductivity experiences a significant drop to a specific value accompanied by a pronounced discontinuity in the transition region, indicates a unique charge transport phenomenon within this composition.

The presence of two different slopes in the Arrhenius plot typically suggests the occurrence of a phase transition or a change in the dominant conduction mechanism within the material. To provide proof of such a transition in BTO, experimental techniques such as differential scanning calorimetry (DSC), dielectric spectroscopy, and impedance spectroscopy can be employed. These techniques can directly measure changes in heat capacity, dielectric permittivity, and conductivity as a function of temperature, providing evidence for phase transitions and changes in conduction mechanisms. For example, dielectric spectroscopy can track changes in dielectric permittivity as a function of temperature, revealing anomalies corresponding to phase transitions. Impedance spectroscopy can characterize the frequency-dependent electrical response of the material, highlighting shifts in conductivity mechanisms across different temperature ranges. By combining these experimental techniques with the analysis of Arrhenius plots, researchers can provide comprehensive evidence for phase transitions and their influence on the electrical properties of BTO and other materials.

3.5 Real permittivity: dielectric constant

The dielectric constant is a fundamental electrical property that characterizes how a material responds to an electric field. It quantifies the ability of a material to store electrical energy when subjected to an electric field. The dielectric properties of BTO can vary significantly with temperature and the presence of impurities or defects. The high dielectric constant of BTO is a result of its ferroelectric behavior, which allows it to exhibit strong polarization and store electrical energy effectively. Binary Ca^{2+} and Mg^{2+} ions-substituted Ba-hexaferrite can affect the dielectric properties of the host material, depending on the type and concentration of the substituted ions. Generally, the dielectric constant of binary ion-substituted Ba hexaferrite is lower compared to materials like BTO. The dielectric constants of these materials play a significant role in their electrical behavior and their suitability for various applications, such as capacitors, dielectric resonators, and microwave devices. Additionally, any alterations in the dielectric constant offer insights into material responses to external influences, rendering it crucial for comprehending and enhancing composite hexaferrite performance in applications like electronics, telecommunications, and electromagnetic devices. The dielectric behavior of these materials is influenced by factors such as the crystallite structure in grains, ion substitution, and microstructure. The 3D representation of the dielectric constant of $(BTO)_{1-x} - (BaMgCaFeO)_x$ $(0.0 \leq x \leq 1.0)$ composite ceramics with varying frequencies and temperatures as presented in Fig. 6 provides a comprehensive understanding of the intricate relationship among composition ratios, temperature, and frequency.

For pure BTO ($x = 0$), a distinctive behavior is observed in the dielectric constant across different temperature ranges and frequencies. Particularly, a pronounced decrease in the dielectric constant at temperatures below 40 °C gives rise to a non-linear trend, wherein the dielectric constant first decreases, reaches a minimum, and subsequently increases as the temperature is raised up to 120 °C. This characteristic evolution is evident within the graph of $x = 0$ presented in Fig. 6. The complex temperature dependence and the presence of this minimum point suggest the involvement of multiple charge carrier mechanisms, phase transitions, or structural changes that influence the dielectric properties [41]. The non-linear variation observed in the dielectric constant of BTO at approximately 40 °C may stem from several factors, including the influence of multiple charge carrier mechanisms, phase transitions, and structural variations on the dielectric properties. However, if this phenomenon is interpreted as a transition, it prompts an exploration into the distinct behavior exhibited at this temperature relative to others, particularly within the framework of an Arrhenius plot. Several potential explanations for this distinct behavior are proposed: Firstly, the transition occurring at approximately 40 °C may necessitate a mechanism differing from transitions observed at other temperatures, potentially involving higher-order phase transitions or the activation of specific energy barriers absent at other temperature regimes. Secondly, there may be coupling effects between various physical properties unique to this temperature range. For instance, variations in grain structure could be correlated with changes in charge carrier mobility or electronic properties, thereby inducing a non-linear trend in the dielectric constant. Thirdly, the proximity of the temperature around

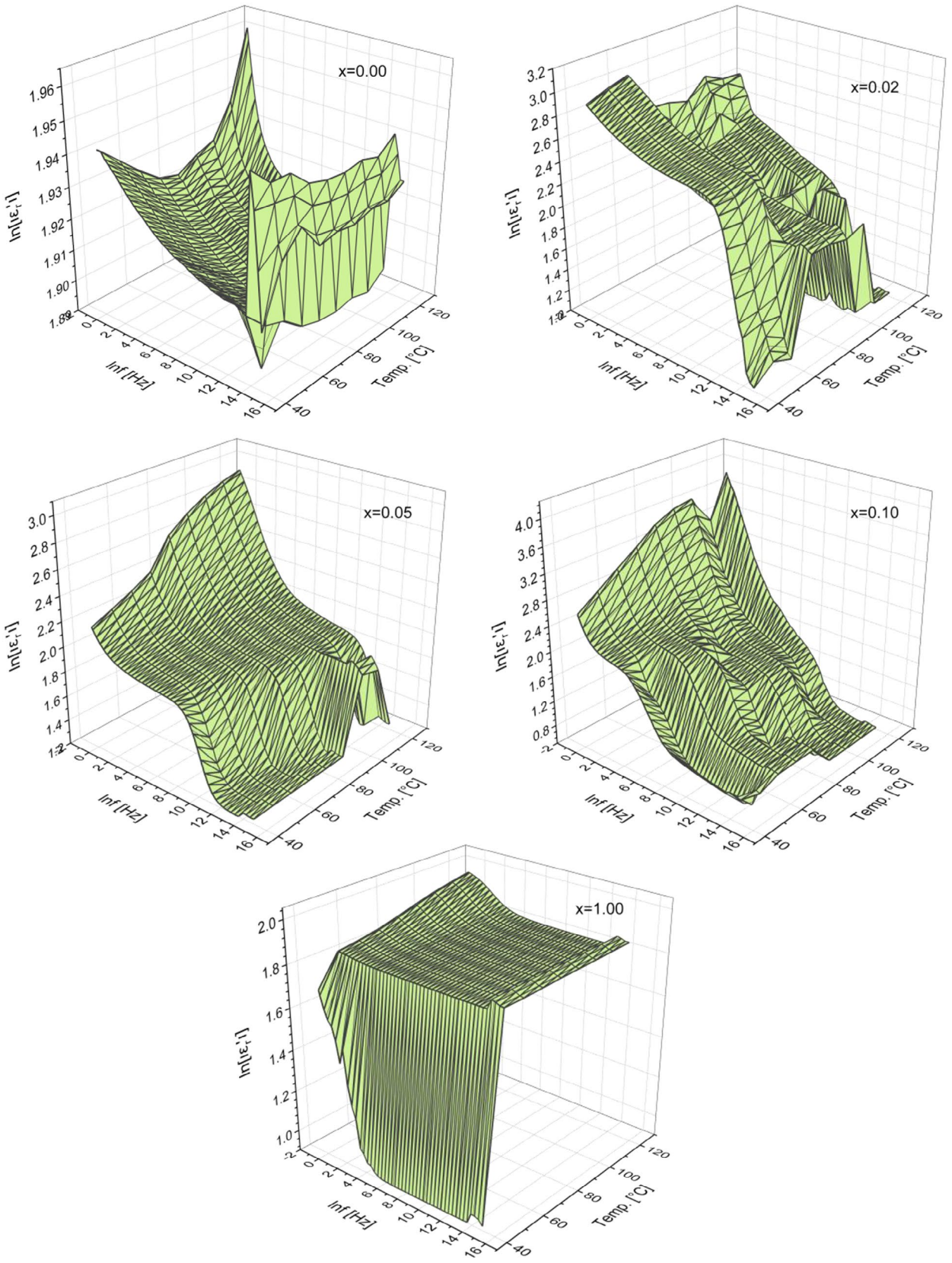


Fig. 6 The 3D representation of the dielectric constant of $(BTO)_{1-x} - (BaMgCaFeO)_x$ $(0.0 \leq x \leq 1.0)$ composite ceramics as functions of frequency and temperature

40 °C to a critical point may initiate substantial alterations in the physical properties of composite ceramics. Near critical points, even slight temperature variations can precipitate significant shifts in the behavior of composite ceramics, resulting in discernible deviations in the dielectric constant. Lastly, defects or impurities within composite ceramics may exhibit heightened activity or exert a substantial influence on the dielectric properties specifically at this temperature range, consequently contributing to the observed non-linear trend. Additional research efforts, incorporating both experimental analyses and computational simulations, are necessary to fully understand the underlying mechanisms driving the observed behavior in the dielectric constant of BTO around 40 °C.

The rapid variation of the dielectric constant with temperature at low frequencies further indicates that the dielectric behavior is sensitive to thermal fluctuations. In the case of the composite ceramic with x = 0.02, fluctuations in the dielectric constant across both frequency and temperature changes reflect the complex nature of the dielectric response. As the proportion of BaCaMgFeO hexaferrite in the $(BTO)_{1-x}$ – $(BaMgCaFeO)_x$ $(0.0 \leq x \leq 1.0)$ composite ceramics is increased, the previously observed fluctuations become less pronounced, and more predictable patterns emerge. However, as the proportion of BaMgCaFeO hexaferrite further increases, as seen in the case of x = 0.10, the impact of temperature on the dielectric constant becomes more dominant, especially at lower frequencies. This effect suggests that the influence of temperature on the dielectric response becomes more pronounced as the composition ratio shifts. A similar trend to BTO is observed in the case of pure BaMgCaFeO hexaferrite ($x = 1$), wherein the dielectric constant increases at lower frequencies, particularly as the temperature surpasses 50 °C. However, at higher frequencies, the dielectric constant remains relatively constant with increasing temperature. This behavior is indicative of the influence of the Ba^{+2} ion in both BTO and BaCaMgFeO hexaferrite composites, particularly in the low-temperature conduction mechanisms. The consistent dielectric response at higher frequencies suggests a decoupling of temperature effects from the frequency-dependent charge carrier dynamics.

Subsequently, the fluctuations in dielectric constant across different composition ratios, temperature ranges, and frequencies highlight the intricate interplay among various charge carrier mechanisms, phase transitions, and the influence of specific ions on the dielectric response. The observed intricate patterns emphasize the multifaceted nature of the dielectric properties within the $(BTO)_{1-x}$ – $(BaMgCaFeO)_x$ composite ceramics. The overarching trends are in line with Maxwell-Wagner polarization and Koop's theory [42–44]. This bodes well for applications like tunable frequency filters and humidity sensors, showcasing consistent responsiveness to changes in composition. Lastly, the dielectric constant of composite hexaferrites signifies their capability to store and transmit electric charge under an electric field. It measures the induced polarization within the material due to electric dipoles. Comprising hexagonal ferrite structures and other components, composite hexaferrites' dielectric constant is affected by factors like structure arrangement, composite composition, and electric field frequency and temperature.

3.6 Imaginary permittivity: dielectric loss

Dielectric loss (or imaginary permittivity) is an important electrical property that characterizes the amount of energy that is lost as heat when a dielectric material is subjected to an alternating electric field. It is a measure of the dissipation of energy due to the interaction between the material's polarization and the applied electric field. The 3D visualization of dielectric loss of $(BTO)_{1-x}$ – $(BaMgCaFeO)_x$ $(0.0 \leq x \leq 1.0)$ composite ceramics as shown in Fig. 7 unravels the intricate relationships among composition ratios, temperature variations, and frequency dependencies.

A key observation emerges when comparing the frequency dependence of dielectric loss for pure BTO (x = 0) and pure BaCaMgFeO hexaferrite ($x = 1$). At temperatures exceeding 50 °C, a common trend is evident, suggesting the influence of shared mechanisms or charge carrier processes that are dominant under these conditions. However, this similarity in behavior changes at lower temperatures, indicating distinct dielectric loss behaviors in different temperature regimes. This transition underscores the complex relationship of mechanisms that contribute to the dielectric response and how these mechanisms evolve as temperature changes. When examining the specific case of $(BTO)_{1-x}$ – $(BaMgCaFeO)_x$ composite ceramics with $x = 0.02$, a distinct pattern of fluctuation in the dielectric loss parameter becomes apparent as both frequency and temperature vary. This behavior reflects the intricate nature of the dielectric response within this composition, suggesting the involvement of multiple interacting factors in shaping the response of the material to external electric fields. The observation of minimum loss values occurring at different frequencies, 7 kHz for BaCaMgFeO hexaferrite and 5 kHz for BTO, highlights the role of the composition ratio in influencing the characteristic frequency at which energy dissipation is minimized. It is important to note that the low-temperature effect observed in the dielectric loss for individual components of the nanocomposites (such as BTO and BaCaMgFeO hexaferrite) is not pronounced within the composition ratios $x = 0.02$, 0.05, and 0.10. This finding implies that the temperature sensitivity of dielectric loss within these ratios

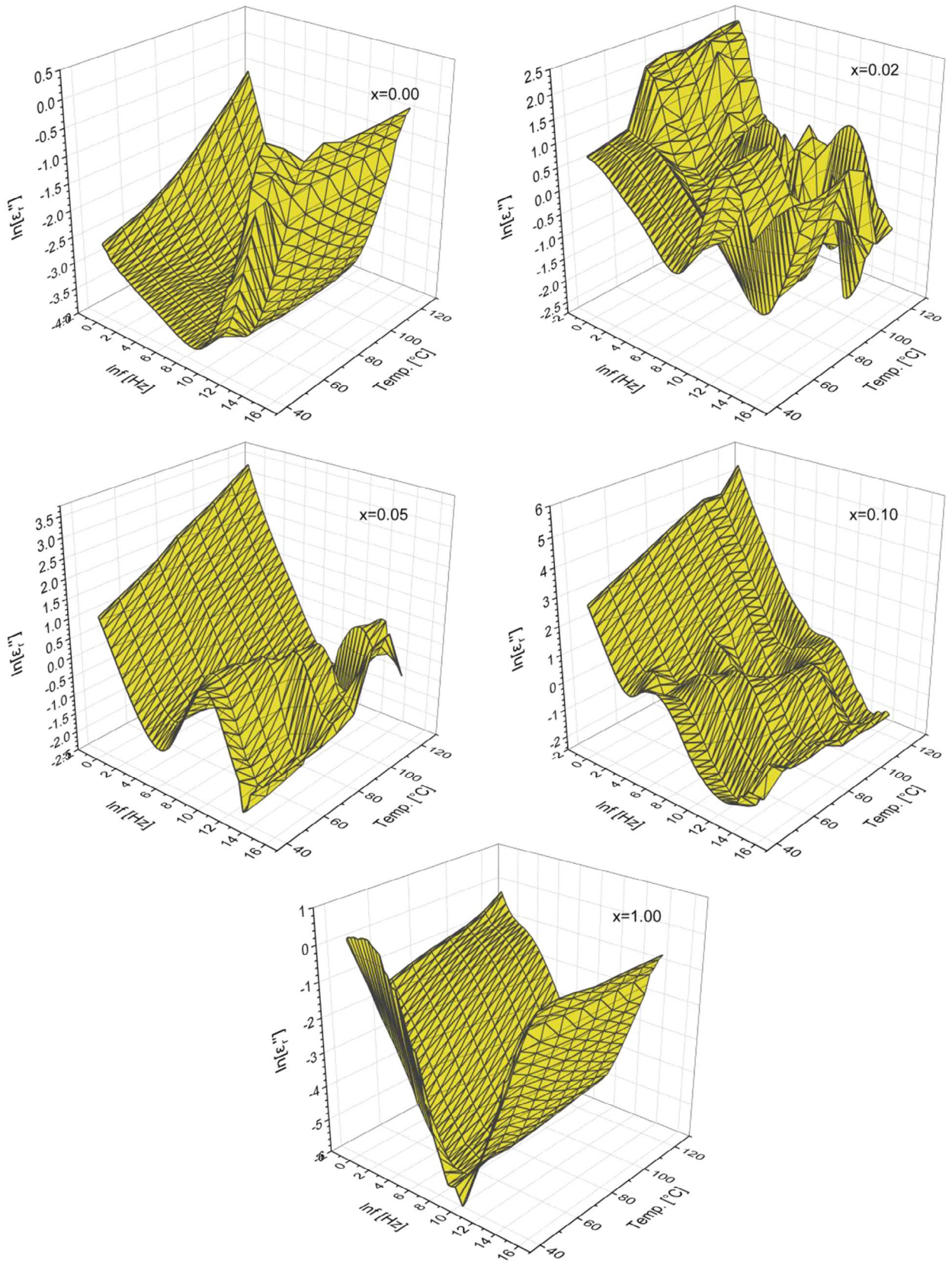


Fig. 7 The 3D representation of dielectric loss of $(BTO)_{1-x}$ – $(BaMgCaFeO)_x$ $(0.0 \leq x \leq 1.0)$ composite ceramics as functions of frequency and temperature

is reduced at lower temperatures. This deviation from the behavior of the individual components underscores the intricate interactions between the constituents that result in unique dielectric loss properties for these intermediate composition ratios.

The temperature dependencies exhibited by $(BTO)_{1-x}$ – $(BaMgCaFeO)_x$ $(0.0 \le x \le 1.0)$ composite ceramics with varying composition ratios underscore the complexity of the relationship among temperature, composition, and dielectric loss behavior. Notably, the influence of the applied electric field on dielectric loss becomes increasingly important as temperature changes, reflecting the coupling between the material's response and external electrical stimulation. The behavior of dielectric loss within $(BTO)_{1-x}-(BaMgCaFeO)_x$ $(0.0 \le x \le 1.0)$ composite ceramics sheds light on the ability of the material to dissipate energy under different conditions and highlights the multifaceted interactions that govern its dielectric performance. Generally, dielectric loss in BTO is a consequence of its ferroelectric polarization and depolarization processes, leading to energy dissipation as heat. The frequency-dependent behavior of dielectric loss in BTO is a result of the phase lag between polarization and the applied field. In BaCaMgFeO hexaferrite, the dielectric loss might be present if there are factors contributing to energy dissipation, but it might not be as significant as in ferroelectric materials. The dielectric loss characteristics of both materials depend on their compositions, crystallite structures in grains, and the interaction between their polarization and the applied electric field. Finally, the dielectric loss in composite hexaferrites involves the dissipation of electrical energy when exposed to alternating electric fields. This energy conversion into heat occurs due to interactions between polarized dipoles and the applied field. In composite hexaferrites, formed by integrating hexagonal ferrite structures with other elements, the extent of dielectric loss is influenced by parameters like composition, intra-grain structure, field frequency, and temperature. Studying and comprehending this loss is pivotal for enhancing performance in applications with energy loss concerns, including electronic components, microwave devices, and electromagnetic shielding.

3.7 Tangential loss: dissipation factor

Dielectric tangent loss is a key parameter that quantifies the energy dissipation in a dielectric material when it is subjected to an alternating electric field. It is a dimensionless quantity that provides insight into how efficiently a material converts electrical energy into heat energy as a result of the dielectric losses. The dielectric tangent loss refers to the ratio of the imaginary component of the complex permittivity (associated with energy dissipation) to the real component (associated with energy storage) when an alternating electric field is applied. As the electric field alternates, the polarization lags behind the changes in the field direction due to the material's inherent response time. This lag between polarization and the applied field leads to energy dissipation and, consequently, dielectric tangent loss. The 3D representation of tangential loss (or dissipation factor) of $(BTO)_{1-x}$ – $(BaMgCaFeO)_x$ $(0.0 \le x \le 1.0)$ composite ceramics as shown in Fig. 8 reveals the complex relationships among composition ratios, temperature fluctuations, and frequency dependencies.

When considering pure BTO (x = 0), the behavior of the tangential loss parameter shows intriguing variations along the logarithmic frequency axis at temperatures below 50 °C. Above this threshold temperature, a distinct shift occurs towards a frequency-independent behavior that increases with temperature up to a frequency of 50 kHz. Subsequently, a pronounced increase at high frequencies is observed for all temperatures exceeding 50 °C. This intricate behavior underscores the dynamic interaction among temperature, frequency, and the ability of the material to dissipate energy. For pure BaMgCaFeO with x = 1, the tangential loss curve reveals two temperature-dependent peaks at different frequencies below 50 °C. As the temperature exceeds this threshold, the frequency dependence of the curve diverges considerably. It demonstrates an initial increase with temperature, followed by a decrease with frequency, a nearly constant mid-frequency region, and a significant increase at high frequencies. This complex behavior suggests the presence of multiple charge carrier mechanisms, phase transitions, or structural transformations that contribute to the tangential loss characteristics within BaCaMgFeO hexaferrite.

The observation that the tangential loss curve for BTO (x = 0) is similar to that of BaCaMgFeO hexaferrite (x = 1) highlights an intriguing commonality in their behavior, despite their compositional differences. However, other composition ratios tend to exhibit distinct patterns in response to both frequency and temperature changes. In the case of $(BTO)_{1-x}$ – $(BaMgCaFeO)_x$ composite ceramic with x = 0.02, the trends appear intricate and fluctuating for both independent variables, underlining the intricate interactions at play. For composition ratios x = 0.05 and 0.10, the tangential loss parameter displays pronounced temperature dependence at low frequencies, while this dependence diminishes at higher frequencies. The presence of peaks at mid and high frequencies in both curves, along with their slight shifts in response to temperature changes, indicates the interplay between frequency-dependent charge carrier mechanisms and their modulation by temperature variations. Remarkably, for $(BTO)_{1-x}$ – $(BaMgCaFeO)_x$ composite ceramics with x = 0.05 and 0.10, the tangential loss parameter consistently exhibits a decrease with frequency,

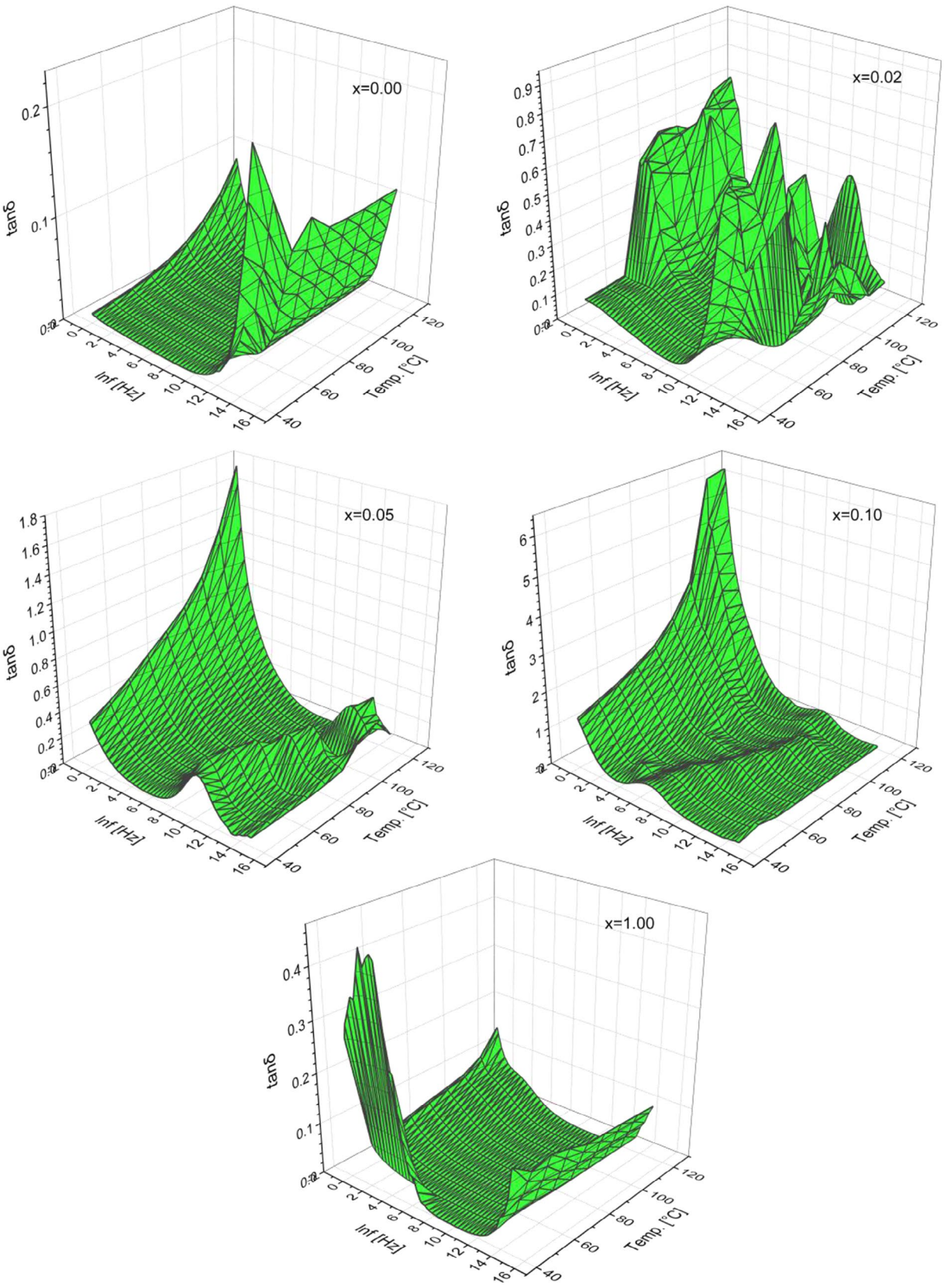


Fig. 8 The 3D representation of tangent loss of $(BTO)_{1-x}$ – $(BaMgCaFeO)_x$ ($0.0 \leq x \leq 1.0$) composite ceramics ($0.0 \leq x \leq 1.0$) as functions of frequency and temperature

coupled with an increase in response to temperature variations. This behavior reflects the influence of both composition ratios and temperature on the dissipation characteristics of these nanocomposites. In summary, the dielectric tangent loss of both BTO and BaCaMgFeO hexaferrite reflects the energy dissipation that occurs as a result of an alternating electric field. In BTO, this loss is related to its ferroelectric polarization behavior, while in BaCaMgFeO hexaferrite, it might be influenced by other factors. The frequency-dependent behavior of dielectric tangent loss in BTO is a result of the phase lag between polarization and the applied field. For BaCaMgFeO hexaferrite, the presence and characteristics of dielectric tangent loss depend on their compositions, crystallite structures in grains, and the nature of interactions within the intra-grains and grain boundaries.

3.8 Complex impedance and dielectric Response: -ImZ/ReZ ratio

Complex impedance is a measure of how a material responds to an alternating electric field. It consists of a real part (resistance or impedance) and an imaginary part (reactance). The analysis of complex impedance, specifically the -ImZ/ReZ ratio, within the context of $(BTO)_{1-x}$ – $(BaMgCaFeO)_x$ $(0.0 \leq x \leq 1.0)$ composite ceramics would provide crucial insights into the capacitive-resistance contribution to the conduction mechanism across varying frequencies, temperatures, and composition ratios (Fig. 9).

For pure BTO (x = 0), distinct trends emerge at different temperature ranges. At lower temperatures (40–50 °C), the impedance ratio curves exhibit peaks at the lowest frequency (6 kHz), while at higher temperatures (> 50 °C), these peaks shift towards higher frequencies. Furthermore, the curves for intermediate temperatures display peaks around 10 kHz, showing slight shifts. These observations highlight the temperature sensitivity of the capacitive-resistance contribution to conduction mechanisms within BTO. In the case of $(BTO)_{1-x}$ – $(BaMgCaFeO)_x$ composite ceramic with x = 0.02, the maximum peak value is observed around 40 kHz at 100 °C, while minimum values are detected at 100 and 120 °C. Notably, the curve at 110 °C exhibits two peaks above 30 kHz, and at 100 °C, the curve displays two peaks at about 6 kHz. This variability in peak positions and magnitudes underscores the complex interplay among frequency, temperature, and composition ratio in shaping the impedance ratio response. For $(BTO)_{1-x}$ – $(BaMgCaFeO)_x$ composite ceramic with x = 0.05, the highest peak value is observed around 30 kHz at 100 °C. Other significant peaks are found around 200 Hz for temperatures between 40 and 70 °C, and they persist up to 9 kHz for temperatures of 80, 90, 110, and 120 °C. Some curves exhibit two distinct peaks—one around 200 Hz and the other around 700 kHz. This intricate pattern suggests that the capacitive-resistance dynamics within the material are influenced by multiple factors, including temperature and composition. In the case of $(BTO)_{1-x}$ – $(BaMgCaFeO)_x$ composite ceramic with x = 0.10, the impedance ratio displays a more complex behavior, with multiple peaks occurring in different frequency domains. Some curves exhibit two peaks with specific shifts, while other peaks show strong composition ratio dependencies in terms of position and magnitude. This behavior signifies the intricate and dynamic interplay of compositional ratios, temperature, and frequency in the contribution of capacitive-resistance to the conduction mechanism. For BaMgCaFeO (x = 1), a systematic measurement reveals strong temperature-dependent behavior of the impedance ratio. The presence of a highest peak at 50 °C and lower peaks at 40 °C underscores the notable temperature sensitivity of the capacitive-resistance dynamics. Furthermore, the peak values exhibit undulating shifts towards higher frequencies with increasing temperature up to 120 °C.

3.9 Cole-Cole analysis: Nyquist plotting

The Cole-Cole analysis is a method used to analyze complex impedance data obtained from dielectric measurements. The analysis of Cole-Cole plot is particularly useful for understanding the frequency-dependent behavior of materials and identifying the presence of different relaxation processes or mechanisms within the material. The Cole-Cole plots for $(BTO)_{1-x}$ – $(BaMgCaFeO)_x$ $(0.0 \leq x \leq 1.0)$ composite ceramics are shown in Fig. 10.

For pure BTO (x = 0), a decrease in frequency from 3.0 MHz reveals a clear trend in the Nyquist plot. The temperature-dependent behavior results in a consistent transition toward a semi-circular arc outside the curve corresponding to T = 30 °C. A notable observation is the capacitive variation dominating the complex impedance, being approximately ten times higher than the resistive response. This suggests that the capacitive contributions significantly influence the overall electrical behavior in BTO. In the case of $(BTO)_{1-x}$ – $(BaMgCaFeO)_x$ composite ceramic with x = 0.02, the Nyquist curves at temperatures between 40 °C and 60 °C exhibit similar linear trends with decreasing frequency. The capacitive-to-resistive ratio remains approximately 10:1, showcasing a nearly temperature-independent variation. However, as temperatures surpass 70 °C, the resistive contribution starts to dominate over the capacitive element in the complex impedance response. For $(BTO)_{1-x}$ – $(BaMgCaFeO)_x$ composite ceramic with x = 0.05, the Nyquist curves display a consistent decrease in impedance with increasing temperature, transitioning into a semi-circular arc shape. The capacitive component decreases across

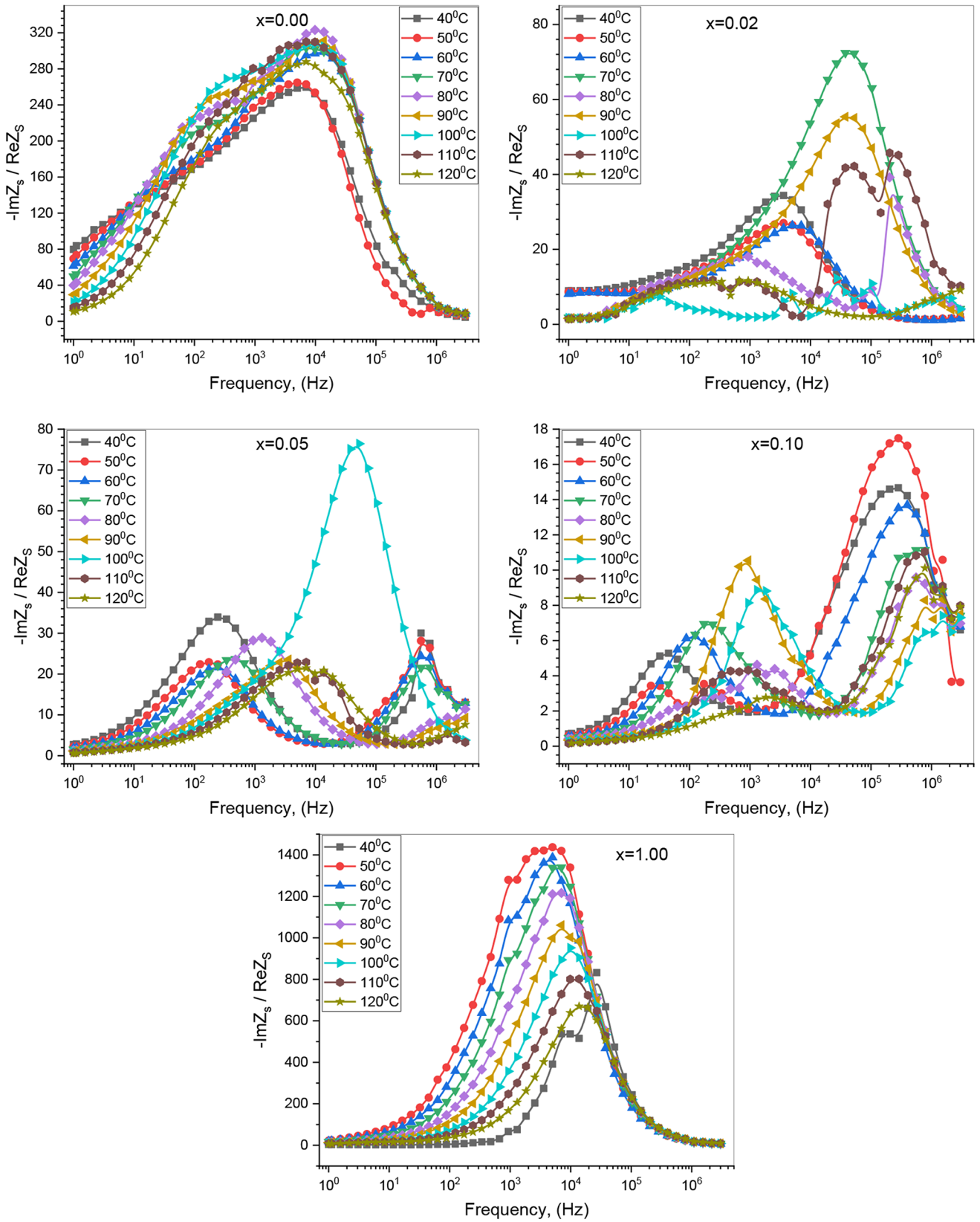


Fig. 9 The *-ImZ/ReZ* ratio of the complex impedance of $(BTO)_{1-x}$ – $(BaMgCaFeO)_x$ $(0.0 \leq x \leq 1.0)$ composite ceramics for varying frequencies up to 3.0 MHz

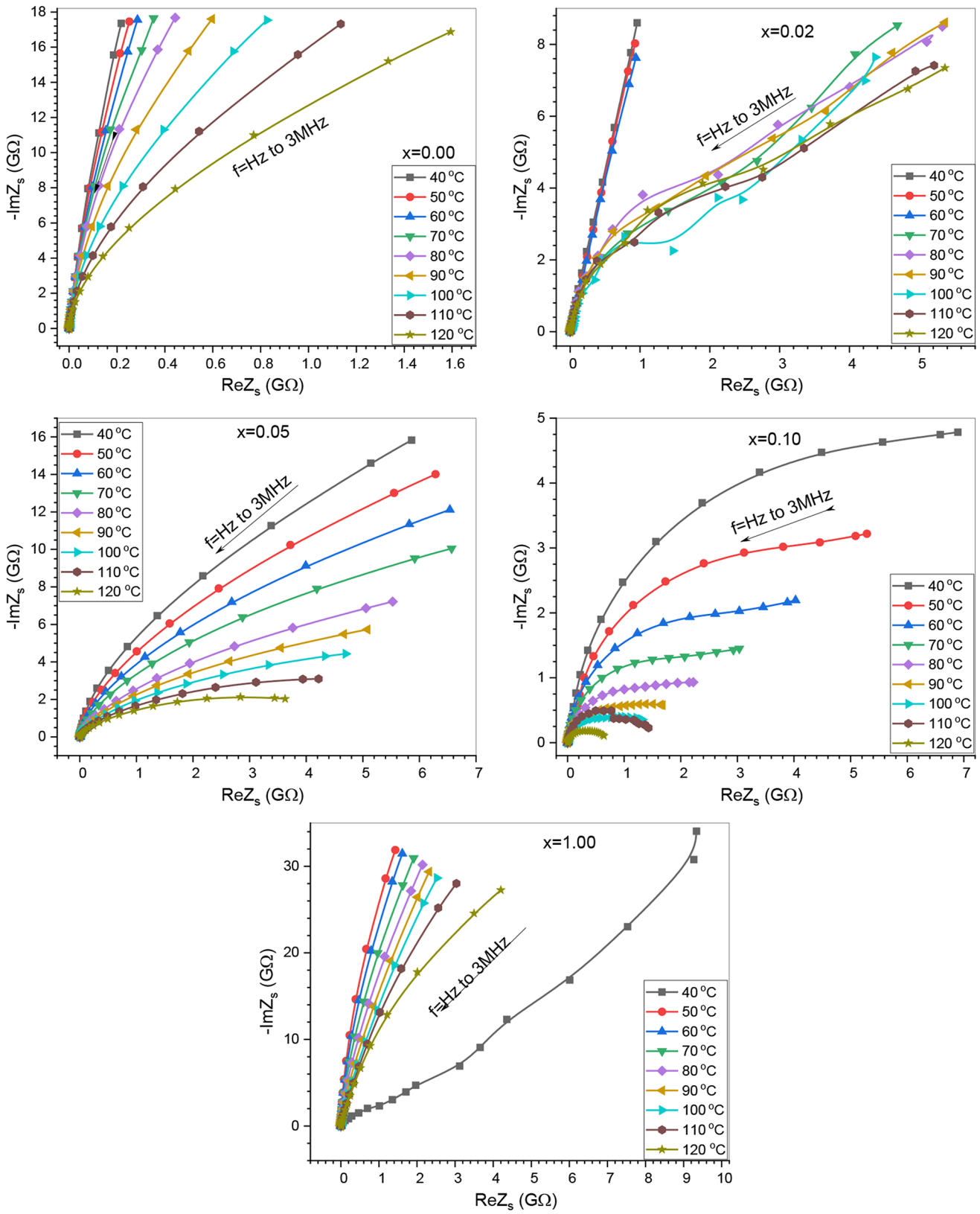


Fig. 10 Nyquist plot of complex impedances of $(BTO)_{1-x}$ – $(BaMgCaFeO)_x$ $(0.0 \leq x \leq 1.0)$ composite ceramics taken between 40 to 120°C up to 3 MHz

the entire temperature range, while the resistive component increases for temperatures below 70 °C and decreases beyond this temperature threshold. In the case of $(BTO)_{1-x}$ – $(BaMgCaFeO)_x$ composite ceramic with x = 0.10, the semi-circular behavior becomes more pronounced as the proportion of BaCaMgFeO hexaferrite in the composite increases. The temperature effect further influences the shape of the Nyquist curves, making them more closely resemble semi-circular arcs. An important observation is the significant reduction in the diameter of the semi-circular arc as temperature increases. Notably, both capacitive and resistive components exhibit a consistent decrease in magnitude with rising temperature. For pure BaCaMgFeO hexaferrite (x = 1.0), the behavior of the Nyquist curves is marked by a notable distinction. A single curve at T = 40 °C stands out from the cluster group curves, suggesting a unique behavior for this specific condition. This deviation cannot be solely attributed to temperature effects. The cluster curves demonstrate regular changes with temperature and frequency, with the resistive component consistently increasing with temperature.

In materials like BTO, the Cole-Cole plot might reveal relaxation processes related to the ferroelectric domains and polarization behaviors. For BaCaMgFeO hexaferrite, the plot could provide information about the relaxation mechanisms associated with the crystallite lattice in grains, defect interactions, or magnetic behavior. Complex materials often exhibit multiple relaxation processes, each corresponding to different charge carrier dynamics or molecular movements. These processes are characterized by additional arcs in the Cole-Cole plot, each with its own center and curvature.

4 Conclusion

In this work, we investigated the temperature-dependent of electrical and dielectric properties of nanocomposites comprising BTO and BaCaMgFeO hexaferrite over various composition ratios using impedance spectroscopy. Parameters like ac/dc conductivity, activation energy, dielectric constant, dielectric loss, dissipation factor, real/imaginary impedance, and Cole-Cole impedance were extensively analyzed. Measurements spanned 3.0 MHz frequency and temperatures from 40 to 120 °C. The ac conductivity adhered to the power law frequency rule, and activation energy (47 to 357 meV) varied due to composition and transition temperatures. Dielectric parameters varied significantly across frequency, temperature, and ratios, reflecting intricate dynamics of intra-grains, grain boundaries, and ionic contributions. Changes in activation energy and dc conductivity stemmed from electron hopping, and ionic contributions, based on composition. Cole-Cole impedance functions highlighted complex resistive and capacitive interactions influenced by intra-grains, grain boundaries, and binary ions. Overall trends aligned with Maxwell-Wagner polarization and Koop's theory. This holds promise for tunable frequency filters and humidity sensors, showing consistent sensitivity to composition changes. The study unraveled multifaceted interactions among composition, temperature, frequency, and electrical attributes in $(BTO)_{1-x}$ – $(BaMgCaFeO)_x$ composite ceramics, revealing complexities in conduction mechanisms and their effects.

Acknowledgements The authors thank Mesut Yildiz from the Faculty of Engineering at Duzce University (Turkey) for his help in performing the scanning electron microscopy analysis.

Author contributions Y. Slimani: Conceptualization, Methodology, Validation, Investigation, Resources, Writing – original draft, Writing – review & editing, Supervision. B. Ünal: Formal analysis, Investigation, Writing – original draft, Writing – review & editing. A. Baykal: Formal analysis, Writing – review & editing. M.A. Almessiere: Formal analysis. A. Thakur: Formal analysis, Investigation. K.M. Batoo: Formal analysis, Investigation.

Funding No funding has been received.

Declarations

Competing interests The authors declare that they have no competing interests.

References

1. H.P. Nagaswarupa, E.T. Mika, H.C.A. Sillanpää, Murthy, Ramachandra, Naik (eds.), *Multifunctional Inorganic Nanomaterials for Energy Applications* (CRC, 2024)
2. Y. Slimani, S.E. Shirsath, H. Erdemi, S.S. Meena, K.M. Batoo, M.A. Almessiere, A. Baykal, A. Thakur, M. Shariq, Improvement in the dielectric, magnetic, ferroelectric, and magnetoelectric coupling attributes of $BaTiO_3/CoNb_{0.02}Fe_{1.98}O_4$ composite systems. Ceram. Int. **50**, 22583–22598 (2024)
3. D. Bochenek, P. Niemiec, D. Brzezińska, G. Dercz, G. Ziółkowski, E. Jartych, J. Grotel, J. Suchanicz, Magnetoelectric properties of Multiferroic composites based on $BaTiO_3$ and Nickel-Zinc Ferrite Material. Materials. **17**, 1905 (2024)
4. J.L.C. Huamán, V.A.G. Rivera, A.H. Pinto, E. Jr. Marega, Multiferroic perovskite ceramics: properties and applications, *In Perovskite ceramics: Recent Advances and Emerging Applications*, Elsevier (2023) 339–381
5. M. Chauhan, E. Arya, A. Kumari, S. Sanghi, A. Agarwal, Structural, magnetic, dielectric, magneto-electric and ferroelectric properties of $BaTiO_3$-$NiFe_2O_4$ multiferroics. J. Alloys Compd. **965**, 171360 (2023)
6. A. Sood, M. Desseigne, A. Dev, L. Maurizi, A. Kumar, N. Millot, S.S. Han, A comprehensive review on barium titanate nanoparticles as a persuasive piezoelectric material for biomedical applications: prospects and challenges. Small. **19**, 2206401 (2023)
7. M. Šuljagić, I. Petronijević, M.M. Mirković, A. Kremenović, A. Džunuzović, V.B. Pavlović, A. Kalezić-Glišović, L. Andjelković, $BaTiO_3/Ni_xZn_{1-x}Fe_2O_4$ (x = 0, 0.5, 1) composites synthesized by

thermal decomposition: magnetic, dielectric and ferroelectric properties. Inorganics. **11**, 51 (2023)
8. S. Pachari, S.K. Pratihar, B.B. Nayak, Microstructure and magnetoresistance driven magnetocapacitance in ex-situ combustion derived $BaTiO_3$-$CoFe_2O_4$ bulk magnetodielectric composites. J. Magn. Magn. Mater. **561**, 169735 (2022)
9. M. Chauhan, A. Agarwal, S. Sanghi, E. Arya, V. Vermani, A. Jangra, S. Kaushik, Crystal structure, dielectric and magnetic properties of $BaTiO_3$–$CoFe_2O_4$ magneto-electric composites, Materials Today: Proceedings 82 (2023) 186–191
10. L. Wang, Q. Lu, X. Lv, Y. Su, Magnetoelectric coupling property of 0–3 type $CoFe_2O_4$-$BaTiO_3$ nanocomposites, Ceram. Int. **49**, 16363–16369 (2023)
11. S. Guiyun, M. Lan, Y. Zhang, S. Zhong, H. Li, C. Chen, K. Ren et al., Enhanced magnetoelectric coupling performance in $CoFe_2O_4$@$BaTiO_3$ multiferroic liquid by tuning the $CoFe_2O_4$ morphology. Mater. Today Commun. **37**, 107423 (2023)
12. P. Dariusz Bochenek, D. Niemiec, G. Brzezińska, Dercz, Grzegorz Ziółkowski, Elżbieta Jartych, Jakub Grotel, Jan Suchanicz, Magnetoelectric Properties of Multiferroic composites based on $BaTiO_3$ and Nickel-Zinc Ferrite Material. Materials. **17**, 1905 (2024)
13. Z. Hasan, H.K. Rouf, M.N.I. Khan, Structural, magnetic, dielectric and electrical properties of $Ba_{0.77}Ca_{0.23}TiO_3$–$Ni_{0.6}Zn_{0.25}La_{0.15}Fe_2O_4$ multiferroic composites. App Phys. A **128**(4), 311 (2022)
14. Y. Gongwen Gan, Z. Yin, Y. Zheng, X. Wang, G. Zhang, Z. Zou, Zhu, Guoqing Gou, two phase $Mg_{0.7}Cd_{0.3}Fe_2O_4$–$BaTiO_3$ composite ceramics with excellent magneto-dielectric properties for antennas in GHz band. Ceram. Int. **49**, 32923–32928 (2023)
15. S.S. Hossain, D. Shekhawat, P.K. Roy, Synthesis and characterization of LTC $x(Ni_{0.90}Mg_{0.10})Fe_2O_4$–$(1-x)(Ba_{0.88}Sr_{0.10}Ca_{0.02})(Ti_{0.95}Zr_{0.05})O_3$ ceramic composites for Antenna Application. Trans. Electr. Electron. Mater. **24**, 528–537 (2023)
16. Y. Slimani, M.A. Almessiere, S.E. Shirsath, E. Hannachi, A. Baykal, N. Alwadai, M.S. Alshatwi, F.N. Almutairi, M. Shariq, K.M. Batoo, A. Thakur, P. Thakur, Impact of $CoFe_{1.98}Nb_{0.02}O_4$ phase on the structural, morphological, and dielectric properties of barium titanate material. Inorg. Chem. Commun. **153**, 110753 (2023)
17. Y. Slimani, R. Sivakumar, S. Meena, R. Vignesh, G. Yasin, E. Hannachi, M.A. Essia, Z. Almessiere, K.M. Trabelsi, A. Batoo, S. Baykal, S. Noureddine, S.E. Brini, I. Shirsath, B. Ercan, Ozcelik, $BaTiO_3$/($Co_{0.8}Ni_{0.1}Mn_{0.1}Fe_{1.9}Ce_{0.1}O_4$) composites: analysis of the effect of $Co_{0.8}Ni_{0.1}Mn_{0.1}Fe_{1.9}Ce_{0.1}O_4$ doping at different concentrations on the structural, morphological, optical, magnetic, and magnetoelectric coupling properties of $BaTiO_3$, Ceram. Int. **48**, 30499 (2022)
18. I. Mohammed, J. Mohammed, A.K. Srivastava, Recent progress in hexagonal ferrites based composites for microwave absorption. Crys Res. Tech. **58**, 2200200 (2023)
19. S. Liu, P. Gao, H. Zou, B. Qin, J. He, L. Deng, Large magnetoelectric effect in $BaFe_{12}O_{19}$-$(Ba_{0.85}Ca_{0.15})(Zr_{0.1}Ti_{0.9})O_3$ particulate composite. Adv. Powder Mater. **1**(3), 100022 (2022)
20. H. Kumar, A. Singh, K. Rana, Effect of substitution on the dielectric and magnetic properties of $BaFe_{12}O_{19}$, in *an introduction to hard ferrites: from fundamentals to practical applications*. Mater. Res. Found. **142**, 66 (2023)
21. A. Kumari, O. Singh, E. Arya, M. Chauhan, V. Vermani, S. Sanghi, A. Agarwal, Crystal structure, dielectric and magnetic properties of $(1-x)$ $BaTiO_3$-(x) $BaFe_{12}O_{19}$ (x = 0.50, 0.60, 0.70) multiferroic composites. App Phys. A **129**, 334 (2023)
22. N. Hooda, R. Sharma, A. Hooda, S. Khasa, Investigations on structure, dielectric and multiferroic behavior of $(1-x)BaFe_{12}O_{19}$–(x) $BaTiO_3$ composites. J. Mater. Sci. : Mater. Electron. **33**, 16441 (2022)
23. Z. Dong, Y. Pu, X. Shi, Y. Hu, P. Wang, Z. Sun, X. Liu, Dielectric properties of (1-x) $BaTiO_3$-x $BaFe_{12}O_{19}$ Composite ceramics. Ferroelectrics. **489**, 1 (2015)
24. M.M. Salem, L.V. Panina, E.L. Trukhanova, M.A. Darwish, A.T. Morchenko, T.I. Zubar, S.V. Trukhanov, Trukhanov, Structural, electric and magnetic properties of $(BaFe_{11.9}Al_{0.1}O_{19})_{1-x}$-$(BaTiO_3)_x$ composites, Compos. B Eng. **174**, 107054 (2019)
25. S. Anand Kumari, A. Sanghi, O. Agarwal, Singh, Investigation of crystal structure, dielectric properties, impedance spectroscopy and magnetic properties of (1-x) $BaTiO_3$–(x) $Ba_{0.9}Ca_{0.1}Fe_{12}O_{19}$ multiferroic composites. Ceram. Int. **47**, 23088–23100 (2021)
26. Z.-Y. Gao, Y.P. Pu, J. Wei, Z.J. Dong, Y. Cui, Enhanced resistivity impact on the magnetoelectric properties of diphase multiferroic $BaTiO_3$–$BaFe_{12-x}Mn_xO_{19}$ composite ceramics. Phys. Status Solidi (RRL). **11**, 1700142 (2017)
27. S.K. Godara, M. Singh, V. Kaur, S.B. Narang, A.K. Sood, Effect of calcium solubility on structural, microstructural and magnetic properties of M-type barium hexaferrite. Ceram. Int. **47**, 20399 (2021)
28. I. Ali, M.U. Islam, M.S. Awan, M. Ahmad, M.A. Iqbal, Structural, electrical, and microstructure properties of nanostructured calcium doped Ba-hexaferrites synthesized by sol-gel method. J. Supercond Nov Magn. **26**, 3277 (2013)
29. M.S. Alam, I. Kagomiya, K. Kakimoto, A comprehensive study of structure, oxygen vacancy, and electrical properties of Mg^{2+} introduced in barium hexaferrite synthesized via spark plasma sintering. J. Solid State Chem. **309**, 122976 (2022)
30. M.A. Almessiere, Y. Slimani, H.S. El Sayed, Baykal, Ca^{2+} and Mg^{2+} incorporated barium hexaferrites: structural and magnetic properties. J. Sol-Gel Sci. Technol. **88**, 628 (2018)
31. C.-C. Huang, C.-C. Mo, Z.-B. Li, Calcination temperature effect on formability and magnetic properties Enhancement of Anisotropic Ca-La-Co substituted M-Type Sr-Hexaferrites Permanent magnets, Mater. Today Commun. **40**, 109444 (2024)
32. R.R.S. Rathore, S. Vijay Desarada, N.B. Chaure, R.K. Pandey, D. Rathore, Enhanced sensitivity towards LPG with selectivity between LPG, NO_2, and NH_3 by novel $CoFe_2O_4$/SiC/$BaTiO_3$ nanocomposites, Ceram. Int. **49**, 16385 (2023)
33. V. Khade, M. Wuppulluri, A comparative study on rigid and flexible magnetoelectric composites. J. Adv. Dielectr. **14**, 2340001 (2024)
34. S. Gaurav, R.K. Kotnala, S. Shankar, A.P. Singh, Dielectric, Impedance, magnetic and Magnetocapacitance investigations in ferrite–manganite nanocomposites for hydroelectric cell applications. Emergent Mater. **7**, 1151–1171 (2024)
35. Y. Slimani, B. Ünal, A. Baykal, M.A. Almessiere, A. Thakur, M. Shariq, Investigation of electrical and dielectric properties of $BaTiO_3$-based composite systems incorporated with various amounts of $Co_{0.8}Mn_{0.1}Ni_{0.1}Fe_{1.9}Ce_{0.1}O_4$. J. Mater. Sci. : Mater. Electron. **35**, 927 (2024)
36. T. Rojac, A. Bencan, G. Drazic, N. Sakamoto, H. Ursic, B. Jancar, G. Tavcar, M. Makarovic, J. Walker, B. Malic, D. Damjanovic, Domain-wall conduction in ferroelectric $BiFeO_3$ controlled by accumulation of charged defects. Nat. Mater. **16**, 322–327 (2017)
37. A.K. Jonscher, The 'universal' dielectric response. Nature. **267**, 673 (1977)
38. Y.A. Zulueta, M.T. Nguyen, M.P. Pham-Ho, Reinvestigation of conducting properties of Ca-doped barium titanate. J. Phys. Chem. Solids. **182**, 111564 (2023)
39. S.S. Hota, D. Panda, R.N.P. Choudhary, Studies of structural, dielectric, conductivity, leakage current mechanism, and efficiency of complex electroceramic. Ceram. Int. **50**, 4031–4045 (2024)
40. B. Ünal, M.A. Almessiere, A. Baykal, Y. Slimani, A. Sadaqat, A. Ul-Hamid, A study on the electrical and dielectric traits of ternary

NiCuZn-spinel ferrites co-substituted with Ga^{3+}-Gd^{3+} ions. Mater. Sci. Eng. B **289**, 116249 (2023)
41. M. Arshad, H. Du, M.S. Javed, A. Maqsood, I. Ashraf, S. Hussain, W. Ma, H. Ran, Fabrication, structure, and frequency-dependent electrical and dielectric properties of Sr-doped $BaTiO_3$ ceramics. Ceram. Int. **46**, 2238 (2020)
42. C.G. Koops, On the dispersion of resistivity and dielectric constant of some semiconductors at audiofrequencies. Phys. Rev. **83**(1), 121 (1951)
43. M. Chauhan, E. Arya, A. Kumari, S. Sanghi, A. Agarwal, Structural, magnetic, dielectric, magneto-electric and ferroelectric properties of $BaTiO_3$-$NiFe_2O_4$ multiferroics. J. Alloy Compd. **965**, 171360 (2023)
44. K. Jyotsna, M. Tomar, S. Phanjoubam, Strong magnetoelectric coupling in novel $Na_{0.5}Bi_{0.5}TiO_3$–$BaFe_{12-2x}Co_xTi_xO_{19}$ multiferroic composite, Ceram. Int. (2024). https://doi.org/10.1016/j.ceramint.2024.06.130

Publisher's Note Springer Nature remains neutral with regard to jurisdictional claims in published maps and institutional affiliations.

Springer Nature or its licensor (e.g. a society or other partner) holds exclusive rights to this article under a publishing agreement with the author(s) or other rightsholder(s); author self-archiving of the accepted manuscript version of this article is solely governed by the terms of such publishing agreement and applicable law.